Electronic Supplementary Material (ESI) for Inorganic Chemistry Frontiers.

Trifluoroacetic Acid Molecules Confined into/onto Metal Organic Frameworks Based on H2btzip for Improving Efficiently Proton Conductivity by the Synergistic Effect

Xiaoxue Ma, [‡a] *Xin Li,* [‡a] *Xueke Han,* [a] *Lu Zhang,* [a] *Ronghua Liu,* [a] *Hongguo Hao,* [a*] *Hui Yan,* [a] *Xin Zhao,* [a] *Xiangjin Kong,* [a] *Huawei Zhou,* [a] *Xia Li,* [a] *Hongjie Zhu,* [a] *Suna Wang,* [a] *Yunwu Li,* [a] *Dichang Zhong,* [b] *Fangna Dai* [c]

[a]Shandong Provincial Key Laboratory of Chemical Energy Storage and Novel Cell Technology, School of Chemistry and Chemical Engineering, and School of Pharmacy, Liaocheng University, Liaocheng 252059, China.

[b]Institute for New Energy Materials and Low Carbon Technologies School of Materials Science and Engineering Tianjin University of Technology Tianjin 300384, China.

[c]College of Science, School of Materials Science and Engineering, China University of Petroleum (East China), Qingdao, Shandong 266580, China.

‡ Xiaoxue Ma [a‡] and Xin Li [a‡] contributed equally to this work.

* Corresponding Authors, E–mail: hhg207@126.com.

Supplementary Information

Contents

1. Materials and Instrumentations.

All reagents and solvents were obtained commercially and used without any purification. Crystal data were obtained from a Rigaku Oxford Diffraction Gemini diffractometer, equipped with a Mo *Kα and* Cu *Kα* with *ω*–scan technique. The powder X–ray diffraction patterns (PXRD) were recorded on a Rigaku D/Max–2500 diffractometer and the intensity data were recorded by continuous scan in a *2θ* mode from 5 to 50°, with a step size of 0.1 and a scan speed of 20 min^{-1}. A PerkinElmer Diamond SII thermal analyser was utilized for Thermo gravimetric analysis (TGA) tests from 298 to 1073 K, at a heating rate of 10 K min^{-1} under a nitrogen atmosphere. A Nicolet 6700 spectrometer was applied to measure the IR spectra in the range 4000–400 cm^{-1}. XPS characterization was carried out by using a Thermo Fisher Scientific ESCALAB spectrometer with Al *Kα* X–rays (1486.6 eV) as the light source.

2. The details information of LCUH–107, LCUH–108, TFA/LCUH–107, and TFA@LCUH–108.

2.1. Synthesis of [Zn(btzip)(H_2O)]·H_2O (LCUH–107). H_2btzip (0.10 mmol, 30.01 mg) and $ZnSO_4·7H_2O$ (0.10 mmol, 28.76 mg) in 10.0 mL deionized water was stirred for 30 min. The mixture was transferred to the Teflon–lined of a 50 mL high pressure stainless steel container and heated at 150 °C for 72 hours, and then cooled to 298 K at the rate of 0.5 °C·min^{-1}. Subsequently, colorless bulk crystals were gathered, washed with ethanol, and dried in vacuum oven. Yield: 65.2% yield based on H_2btzip. IR (KBr pellet: cm^{-1}): 3545(s), 3422(s), 3121(s), 3089(w), 1629(s), 1530(s), 1381(s), 1282(m), 1211(w), 1141(w), 977(m), 909(w), 656(m), 586(w).

2.2. Synthesis of [Ni(btzip)(H_2btzip)] (LCUH–108). H_2btzip (0.10 mmol, 30.01 mg) and $NiCl_4·6H_2O$ (0.20 mmol, 47.52 mg) in 8.0 mL DMF and 8.0 mL acetonitrile was stirred for 30 min. The mixture was transferred to the Teflon–lined of a 50 mL high pressure stainless steel container and heated at 150 °C for 72 hours, and then cooled to 298 K at the rate of 0.5 °C·min^{-1}. Subsequently, blue sheet–like crystals were gathered, washed with ethanol, and dried in vacuum oven. Yield: 54.7% yield based on H_2btzip. IR (KBr pellet: cm^{-1}): 3131(w), 1663 (w), 1529 (w), 1387 (s), 1134 (s), 976 (m), 653 (m), 448(w).

2.3. Synthesis of TFA/LCUH–107. The activated 100 mg **LCUH–107** was immerged in V_{TFA} : V_{MT} = 1 : 40, 1 : 30, 1 : 20, 1 : 10 (V : V) solution of 10.0 mL for 1 h. The crystal was then dried under vacuum oven at 70 °C to obtain the trifluoroacetic acid–supported product TFA@**LCUH–107**.

2.4. Synthesis of TFA@LCUH–108. The activated 100 mg **LCUH–108** was immerged in V_{TFA} : V_{MT} = 1 : 20, 1 : 15, 1 : 10, 1 : 5 (V : V) solution of 10.0 mL for 1 h. The crystal was then dried under vacuum oven at 70 °C to obtain the trifluoroacetic acid–supported product TFA@**LCUH–108**.

3. Crystal structure of LCUH–107.

Table S1. Crystal Parameters for **LCUH–107**.

Complex	**LCUH–107**
CCDC no.	2202297
Formula	$C_{12}H_{10}N_6O_6Zn$
Mr	399.63
Temperature/K	298.15
Crystal system	monoclinic
space group	*P21/c*
a (Å)	10.2034(8)
b (Å)	16.0013(13)
c (Å)	8.7996(7)
α, β, γ/°	90, 98.18 (3),90
V/Å^3	1422.1(2)
Z	4
D calcd (g cm^{-3})	1.867
μ (mm^{-1})	1.777
F(000)	808.0
Reflections collected	6647

R_{int}	0.0494
Goodness of fit	1.052

Table S2. Selected Bond Lengths (Å) of **LCUH–107.**

LCUH–107	
Atom–Atom	**Length/Å**
N6–Zn1[1]	2.140(3)
O5–Zn1	2.015(3)
O1–Zn1[2]	1.966(3)
O4–Zn1[3]	2.074(3)
Zn1–N1	2.063(3)

Table S3. Selected bond angles (º) for **LCUH–107**.

LCUH–107	
Atom–Atom– Atom	**Angle/°**
O5–Zn1–N6[4]	85.08(12)
O5–Zn1–O4[5]	88.82(11)
O5–Zn1–N1	116.98(13)
O1[6]–Zn1–N6[4]	97.00(12)
O1[6]–Zn1–O5	141.51(13)
O1[6]–Zn1–O45	88.05(11)
O1[6]–Zn1–N1[2]	87.64(6)
O4[5]–Zn1–N6[4]	173.41(6)
N1–Zn1–N6[4]	95.15(12)
N1–Zn1–O4[5]	87.21(12)
C9–N1–Zn1	136.6(2)
C10–N1–Zn1	120.2(3)
C8–O4–Zn1[3]	132.2(3)
C7–O1–Zn1[2]	125.8(3)
C1[1]–N6–Zn1[1]	126.2(3)

C1²–N6–Zn1¹	129.6(3)

Table S4. Crystal Parameters for **LCUH–108**.

Complex	**LCUH–108**
CCDC no.	2297919
Formula	$C_{24}H_{14}N_{12}O_8Ni$
Mr	657.18
Temperature/K	298.15
Crystal system	Orthorhombic
space group	*Pbcm*
a (Å)	7.2370(8)
b (Å)	20.4549(19)
c (Å)	24.962(2)
α, β, γ/°	90, 90,90
V/Å³	3695.2(6)
Z	13
D calcd (g cm^{-3})	1.181
μ (mm^{-1})	0.579
F(000)	1336
Reflections collected	3348
Goodness of fit	1.012

Table S5. Selected Bond Lengths (Å) of **LCUH–108**.

LCUH–108	
Atom–Atom	**Length/Å**
N6–Ni1	2.088(7)
O2–Ni1	2.093(5)
N3–Ni1	2.103(7)

Table S6. Selected bond angles (º) for **LCUH–108**.

LCUH–108	
Atom–Atom– Atom	**Angle/°**
N6^{1}–Ni^{1}–N6	180.0(4)
N6^{1}–Ni^{1}–O2^{2}	85.6(2)
N6–Ni1–O2^{2}	94.4(2)
N6^{1}–Ni1–O2^{3}	94.4(2)
N6–Ni1–O2^{3}	85.6(2)
O2^{2}–Ni1–O2^{3}	180.0
N6^{1}–Ni1–N3	93.2(3)
N6–Ni1–N3	86.8(3)
O2^{2}–Ni1–N3	88.7(2)
O2^{3}–Ni1–N3	91.3(2)
N6^{1}–Ni1–N3^{1}	86.8(3)
N6–Ni1–N3^{1}	93.2(3)
O2^{2}–Ni1–N3^{1}	91.3(2)
O2^{3}–Ni1–N3^{1}	88.7(2)
N3–Ni1–N3^{1}	180.0
C16–N3–Ni1	129.2(6)
C17–N3–Ni1	127.7(6)
C8–O2–Ni3^{6}	132.1(5)
C1–N6–Ni1	124.1(6)
C21–N6–Ni1	130.1(6)

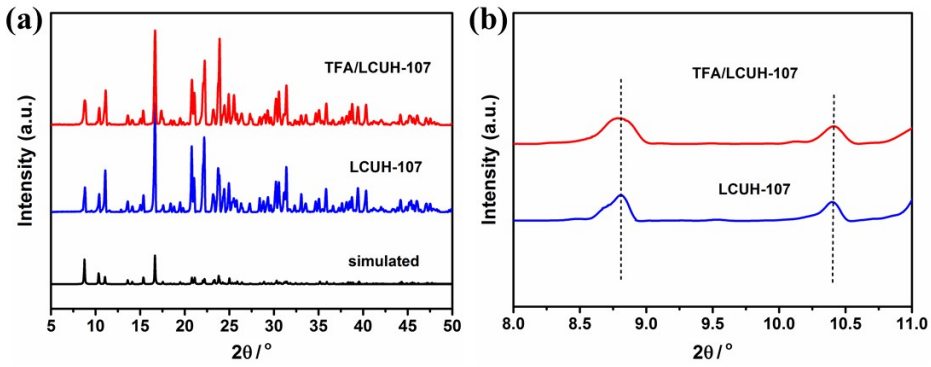

Figure S1. (a) and (b) The simulated PXRD pattern of **LCUH–107** (black line) and PXRD patterns of synthesized **LCUH–107** sample (red line) and TFA/**LCUH–107** sample (blue line).

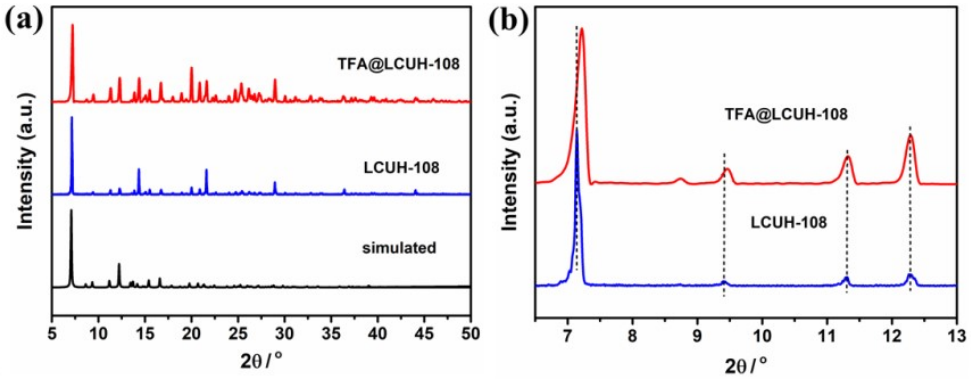

Figure S2. (a) and (b) The simulated PXRD pattern of **LCUH–108** (black line) and PXRD patterns of synthesized **LCUH–108** sample (red line) and TFA@**LCUH–108** sample (blue line).

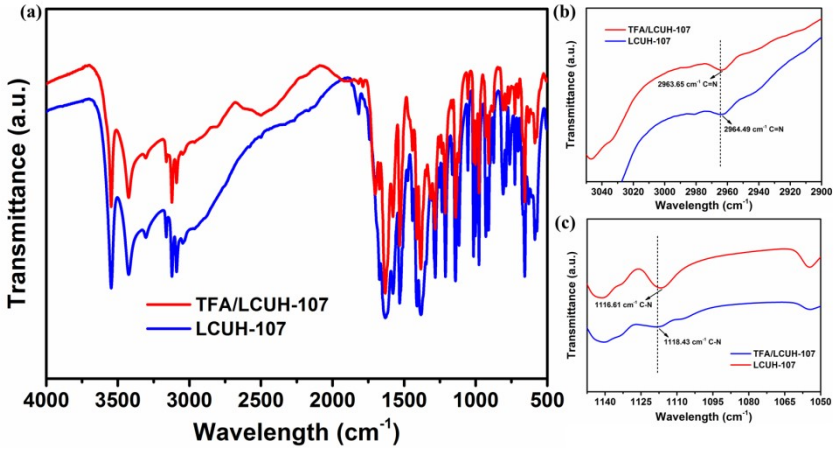

Figure S3. (a), (b), and (c) IR spectra (KBr pellet, cm^{-1}) of **LCUH–107** (blue line) and TFA/**LCUH–107** (red line).

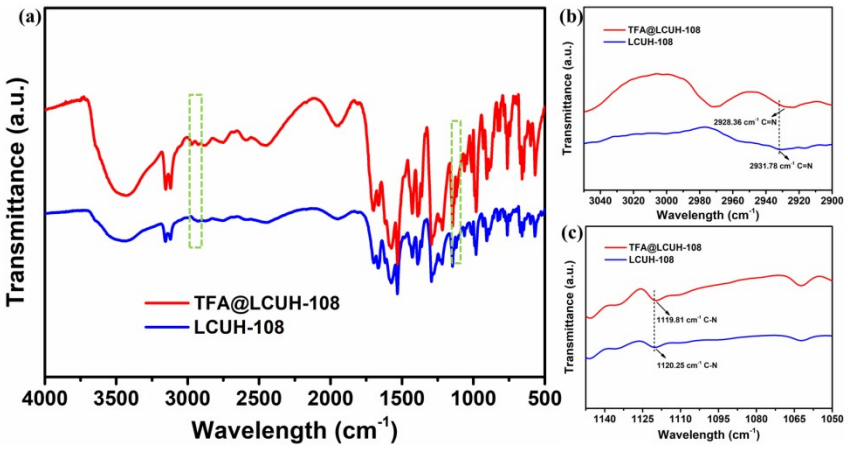

Figure S4. (a), (b), and (c) IR spectra (KBr pellet, cm^{-1}) of **LCUH–108** (blue line) and TFA@**LCUH–108** (red line).

4. AC Impedance Analysis.

The 80–100 mg sample was put into the customized mold of 10 mm × 4 mm and pressed under 2 MPa pressure for 3 min to make the cuboid sample block. The size of the cuboid sample block was accurately measured by the vernier caliper. Apply silver glue to both sides of the cuboid sample block and connect them to the latex sample table with silver wire. The sample stand is then placed in a custom–made double glass bottle and sealed at a certain temperature controlled by a high–temperature circulation tank. The AC impedance spectra were tested on CHI–760E electrochemical workstation with a frequency range of 1 Hz to 1 MHz and signal amplitude of 200 mV. Impedance spectra at different temperatures and relative humidities were recorded where the relative humidities were controlled by standard saturated aqueous solutions of different salts.

The proton conductivity values were calculated by the following equation:

$$\sigma = \frac{l}{RS} \qquad (1)$$

where σ is the proton conductivity ($S \cdot cm^{-1}$), l is the length (cm) of the cube, S is the area covered with silver glue (cm^2) and R is the bulk resistance (Ω).

The activation energy (E_a) was calculated by the following equation:

$$\ln \sigma_T = \ln \sigma_0 - \frac{E_a}{KT} \qquad (2)$$

where σ is the proton conductivity ($S \cdot cm^{-1}$), σ_0 is the preexponential factor, K is the Boltzmann constant (eV/K), and T is the temperature (K).

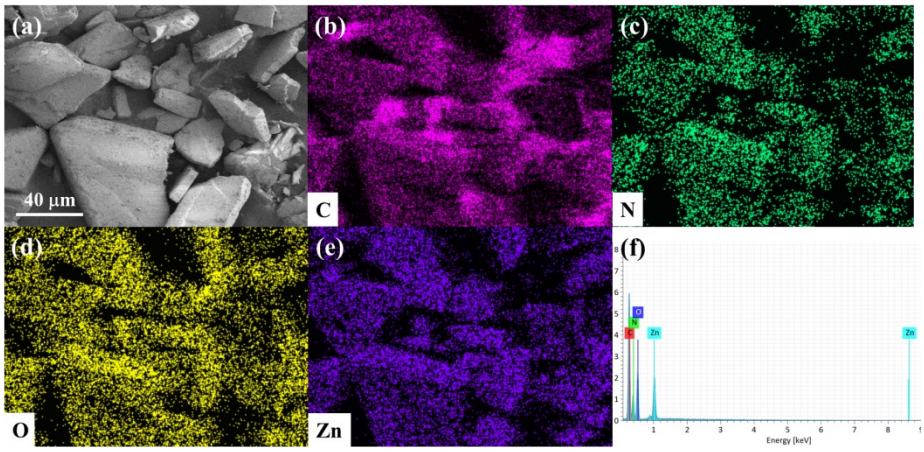

Figure S5. SEM image of **LCUH–107** (a); energy–dispersive elemental mapping images for **LCUH–107**: C (b), N (c), O (d), and Zn (e); EDS image of **LCUH–107** (f).

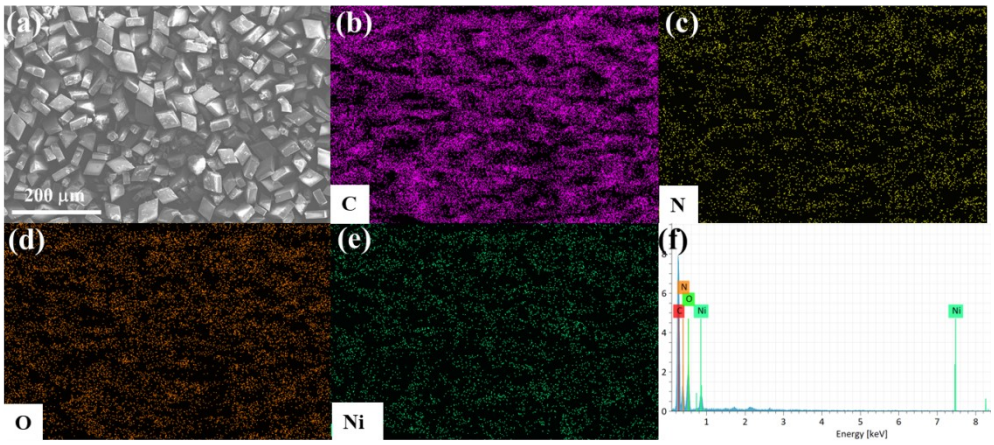

Figure S6. SEM image of **LCUH–108** (a); energy–dispersive elemental mapping images for **LCUH–108**: C (b), N (c), O (d), and Ni (e); EDS image of **LCUH–108** (f).

Table S7. The conductivity values ($S \cdot cm^{-1}$) of TFA/**LCUH–107** by different volume ratios of trifluoroacetic acid (TFA) and methanol (MT) under 100% RH and 80 °C.

$V_{TFA} : V_{MT}$	1 : 10	1 : 20	1 : 30	1 : 40
$\sigma(10^{-2}\ S \cdot cm^{-1})$	3.00	2.95	1.33	1.16

The effect of different volume ratios of trifluoroacetic acid (TFA) to methanol (MT) on the proton conductivity of TFA/**LCUH–107** was determined. For TFA/**LCUH–107**, when the volume ratios of TFA and MT ($V_{TFA} : V_{MT}$) are 1 : 40, 1 : 30, 1 : 20, and 1 : 10, the conductivities of TFA/**LCUH–107** are 1.16×10^{-2}, 1.33×10^{-2}, 2.95×10^{-2}, and 3.00×10^{-2}

$S \cdot cm^{-1}$, respectively. When V_{TFA} : V_{MT} from 1 : 20 to 1 : 10, the conductivity of TFA/**LCUH–107** increases only a little (5.0×10^{-4} $S \cdot cm^{-1}$). Therefore, from the aspects of cost and conductivity, we selected the values of V_{TFA} : V_{MT} of 1 : 20 to synthesize TFA/**LCUH–107** for experimental investigation.

Table S8. The conductivity values ($S \cdot cm^{-1}$) of TFA@**LCUH–108** by different volume ratios of trifluoroacetic acid (TFA) and methanol (MT) under 100% RH and 80 °C.

V_{TFA} : V_{MT}	1 : 5	1 : 10	1 : 15	1 : 20
σ(10^{-1} S·cm^{-1})	2.02	2.05	0.88	0.59

Similarly, the effect of different volume ratios of trifluoroacetic acid (TFA) to methanol (MT) on the proton conductivity of TFA@**LCUH–108** was determined. For TFA@**LCUH–108**, when the volume ratios of TFA and MT (V_{TFA} : V_{MT}) are 1 : 20, 1 : 15, 1 : 10, and 1 : 5, the conductivities of TFA@**LCUH–108** are 5.90×10^{-2}, 8.80×10^{-2}, 2.05×10^{-1}, and 2.02×10^{-1} $S \cdot cm^{-1}$, respectively. When V_{TFA} : V_{MT} from 1 : 10 to 1 : 5, the conductivity change of TFA@**LCUH–108** is negligible. Therefore, from the aspects of cost and conductivity, we selected the values of V_{TFA} : V_{MT} of 1 : 10 to synthesize TFA@**LCUH–108** for experimental investigation.

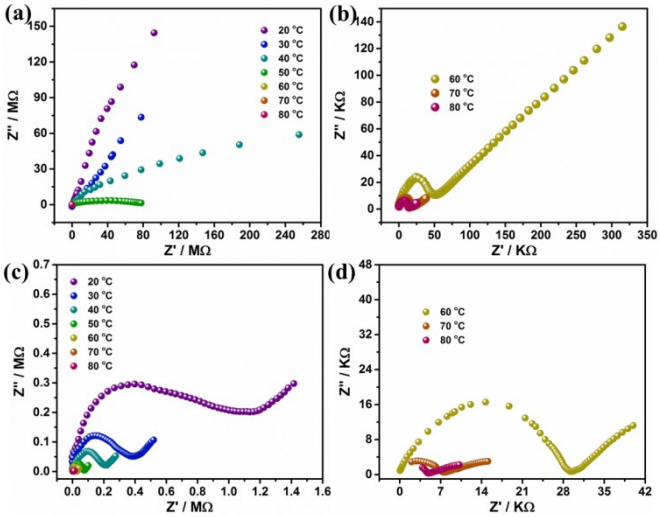

Figure S7. Impedance spectra of **LCUH–107** (a) and (b), and TFA/**LCUH–107** (c) and (d) at 45% RH.

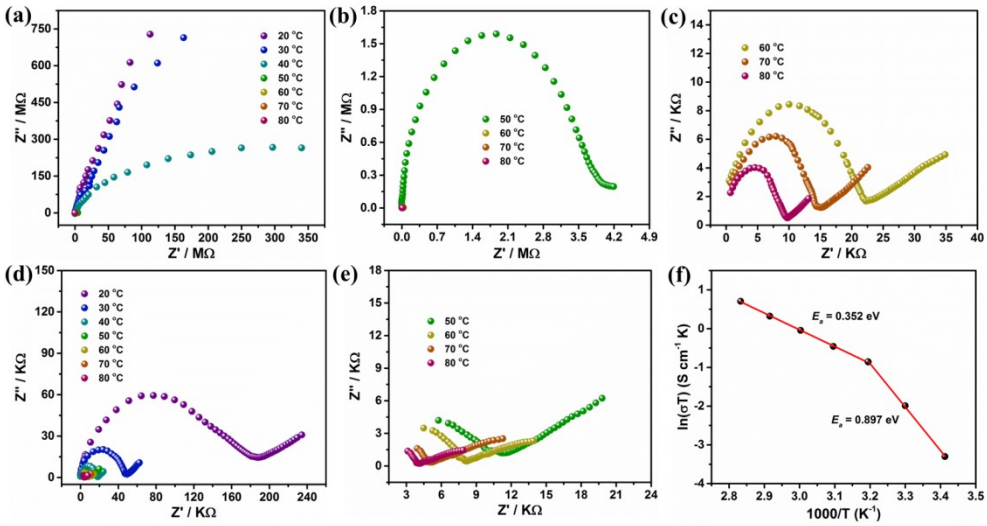

Figure S8. Impedance spectra of **LCUH–107** (a), (b), and (c) and TFA/**LCUH–107** (d) and (e) at 60% RH (c); Arrhenius plots of proton conductivities for TFA/**LCUH–107** (f) at 60% RH.

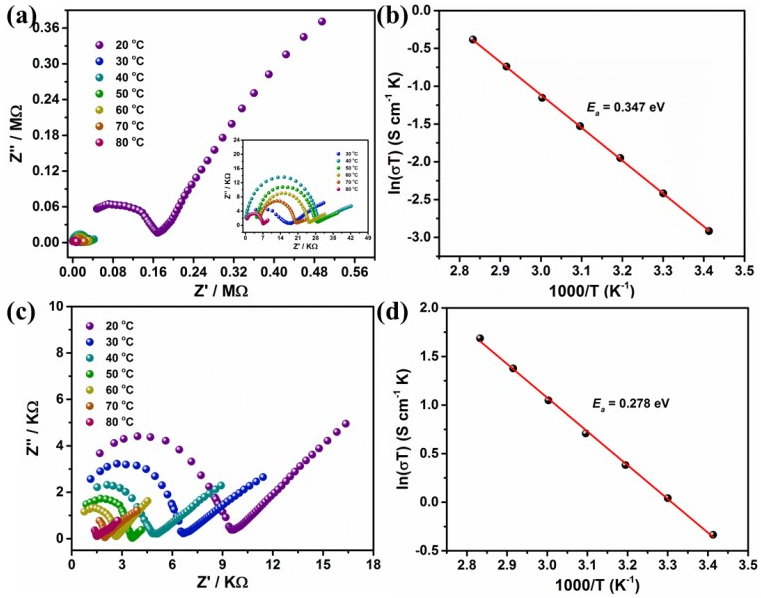

Figure S9. Impedance spectra of **LCUH–107** (a) and TFA/**LCUH–107** (c) at 75% RH; Arrhenius plots of proton conductivities for **LCUH–107** (b) and TFA/**LCUH–107** (d) at 75% RH.

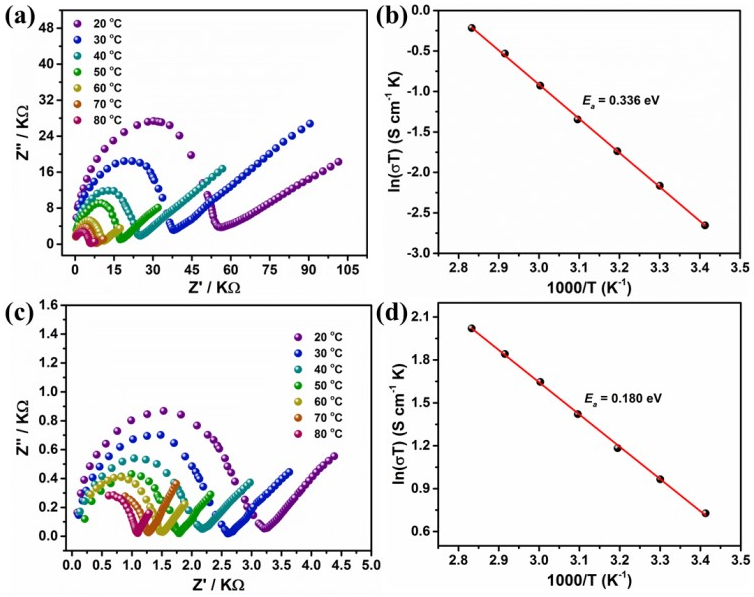

Figure S10. Impedance spectra of **LCUH–107** (a) and TFA/**LCUH–107** (c) at 85% RH; Arrhenius plots of proton conductivities for **LCUH–107** (b) and TFA/**LCUH–107** (d) at 85% RH.

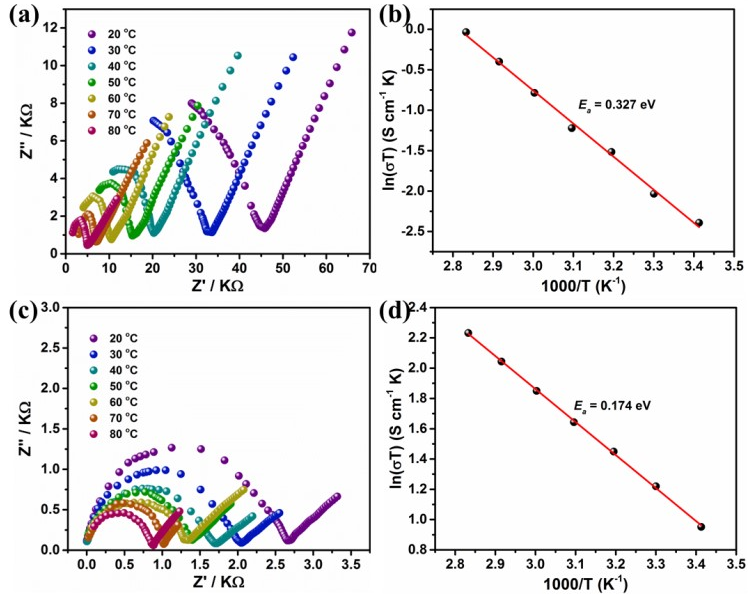

Figure S11. Impedance spectra of **LCUH–107** (a) and TFA/**LCUH–107** (c) at 93% RH; Arrhenius plots of proton conductivities for **LCUH–107** (b) and TFA/**LCUH–107** (d) at 93% RH.

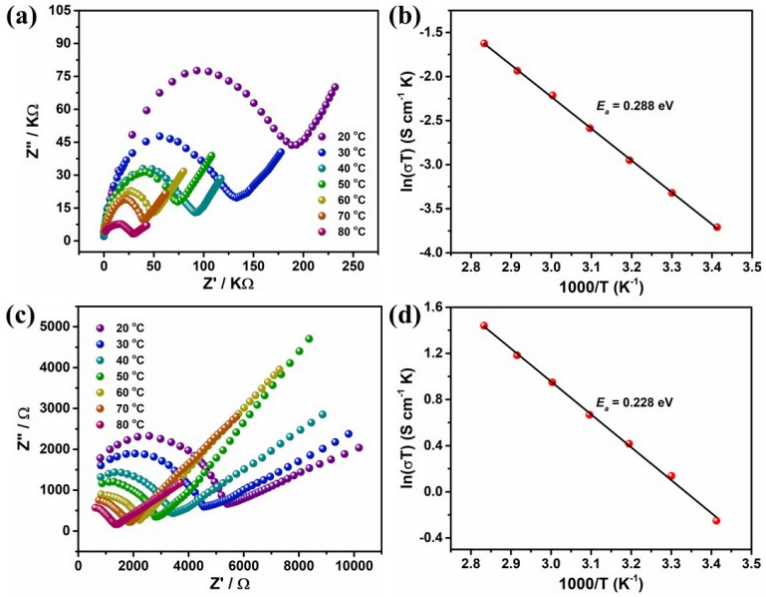

Figure S12. Impedance spectra of **LCUH–108** (a) and TFA@**LCUH–108** (c) at 45% RH; Arrhenius plots of proton conductivities for **LCUH–108** (b) and TFA@**LCUH–108** (d) at 45% RH.

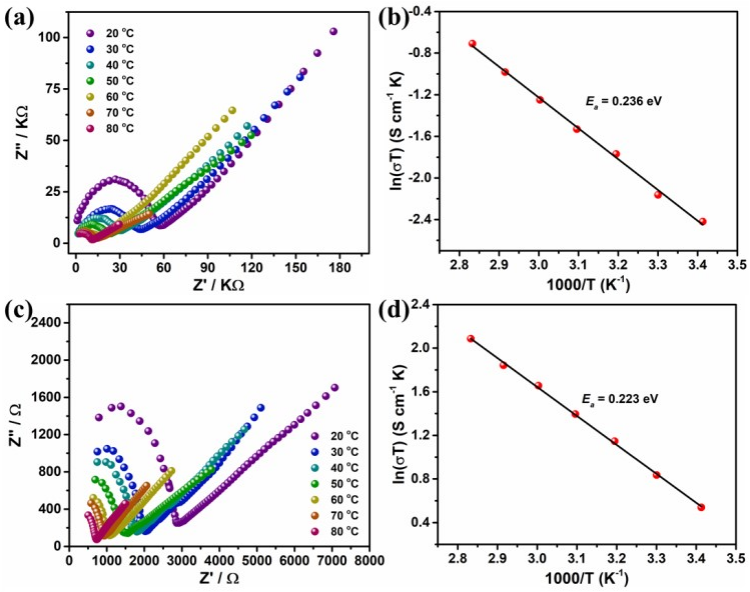

Figure S13. Impedance spectra of **LCUH–108** (a) and TFA@**LCUH–108** (c) at 60% RH; Arrhenius plots of proton conductivities for **LCUH–108** (b) and TFA@**LCUH–108** (d) at 60% RH.

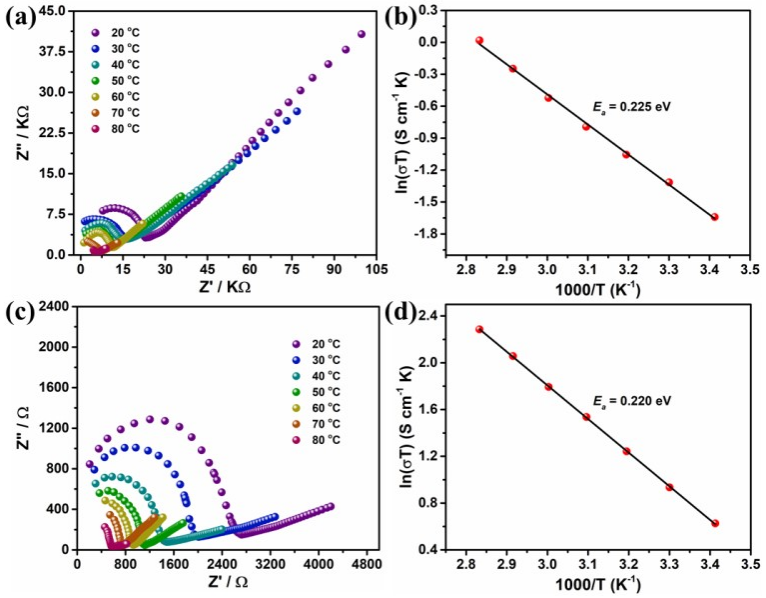

Figure S14. Impedance spectra of **LCUH–108** (a) and TFA@**LCUH–108** (c) at 75% RH; Arrhenius plots of proton conductivities for **LCUH–108** (b) and TFA@**LCUH–108** (d) at 75% RH.

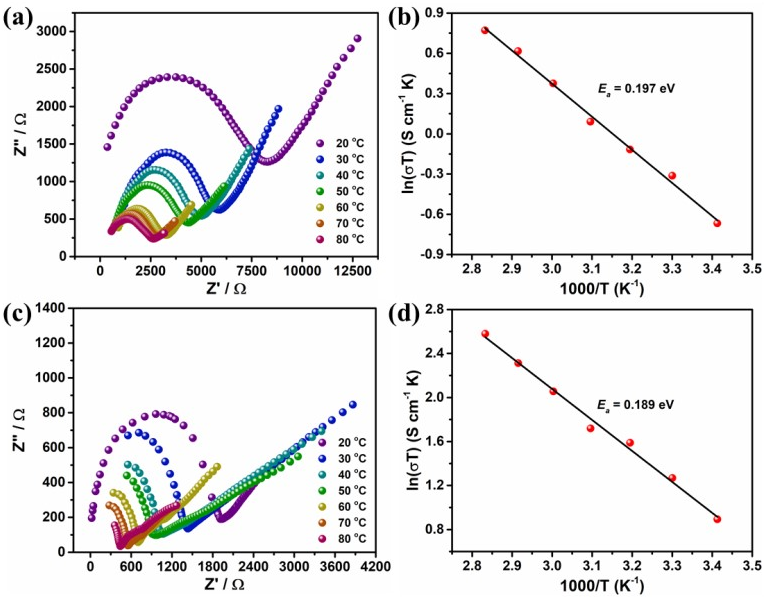

Figure S15. Impedance spectra of **LCUH–108** (a) and TFA@**LCUH–108** (c) at 85% RH; Arrhenius plots of proton conductivities for **LCUH–108** (b) and TFA@**LCUH–108** (d) at 85% RH.

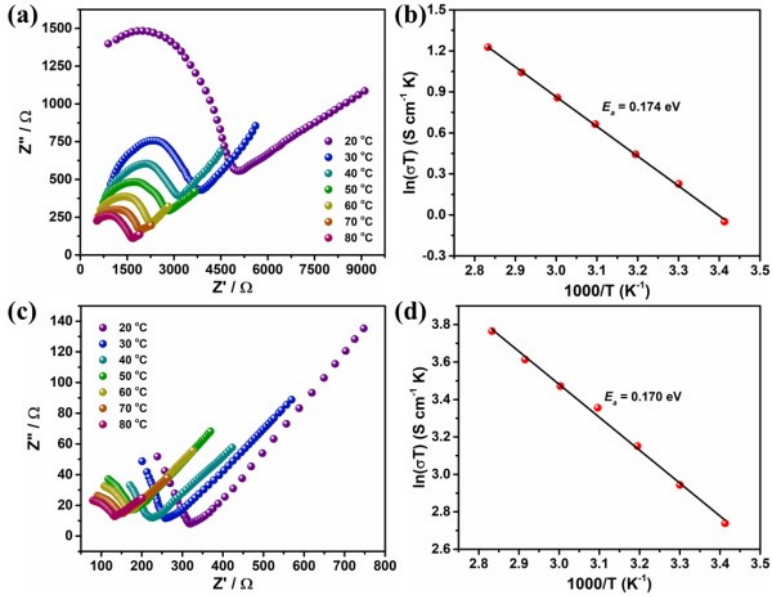

Figure S16. Impedance spectra of **LCUH–108** (a) and TFA@**LCUH–108** (c) at 93% RH; Arrhenius plots of proton conductivities for **LCUH–108** (b) and TFA@**LCUH–108** (d) at 93% RH.

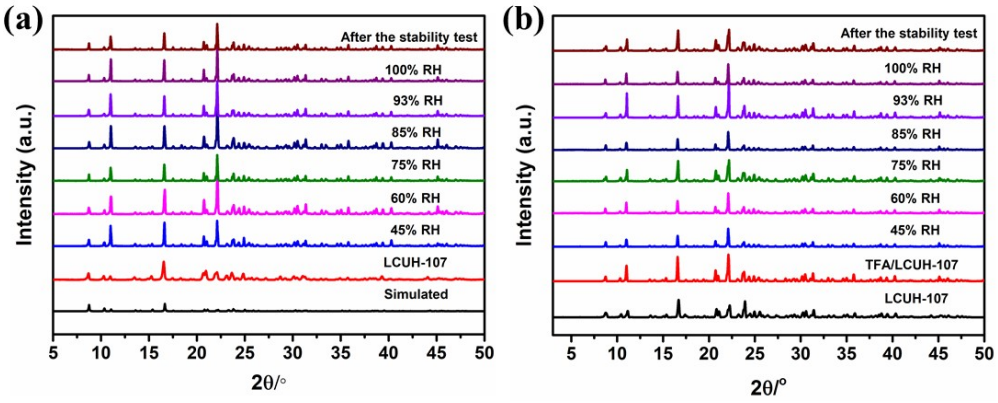

Figure S17. PXRD patterns of **LCUH–107** (a) and TFA/**LCUH–107** (b): as–synthesized, after impedance measurements and after stability tests.

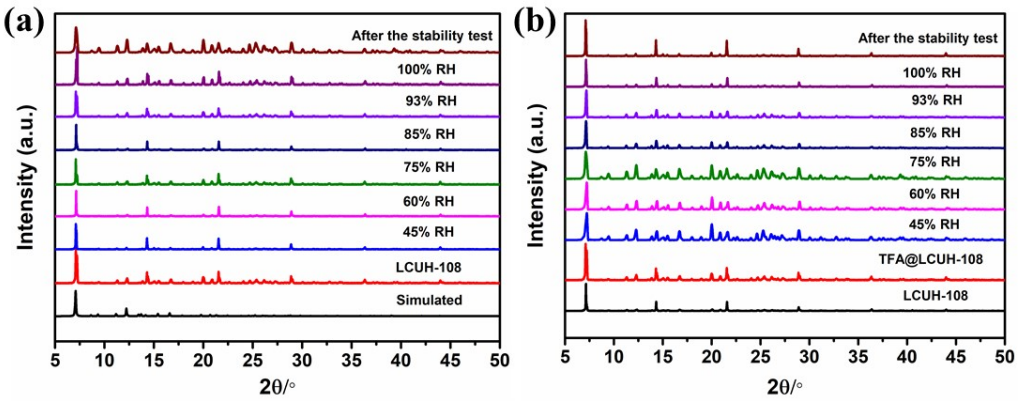

Figure S18. PXRD patterns of **LCUH–108** (a) and TFA@**LCUH–108** (b): as–synthesized, after impedance measurements and after stability tests.

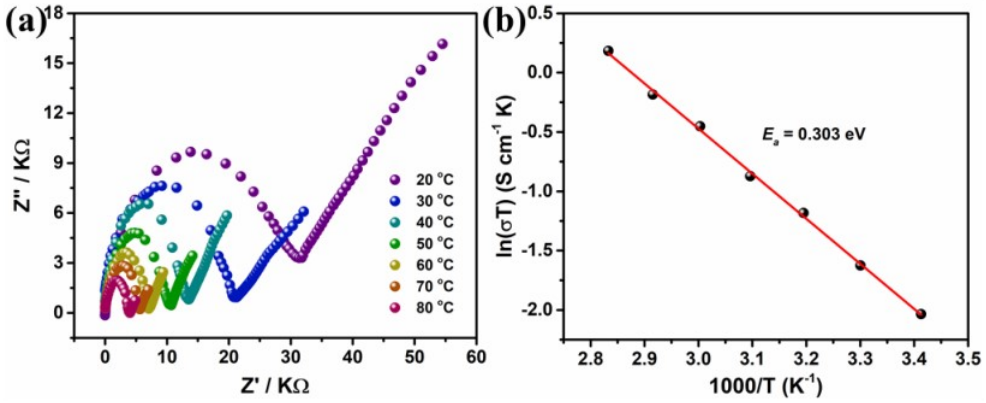

Figure S19. (a) Impedance spectra of TFA/**LCUH–107W** at 100% RH; (b) Arrhenius plots of proton conductivities for TFA/**LCUH–107W** at 100% RH.

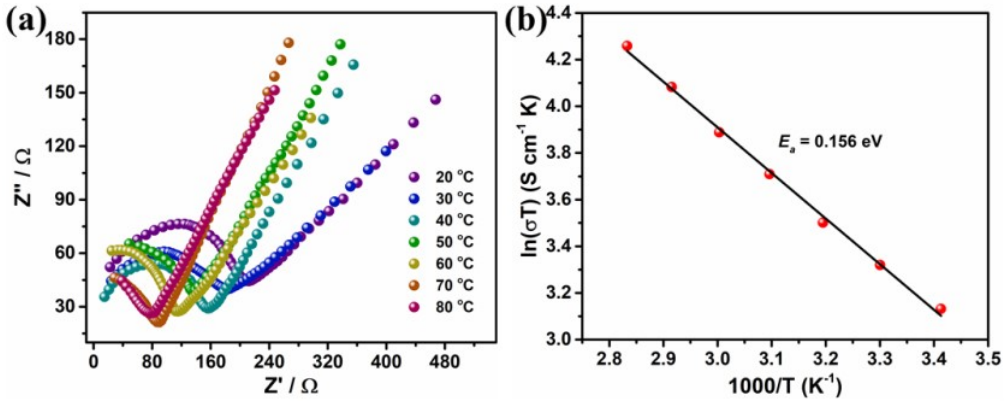

Figure S20. (a) Impedance spectra of TFA@**LCUH–108W** at 100% RH; (b) Arrhenius plots of proton conductivities for TFA@**LCUH–108W** at 100% RH.

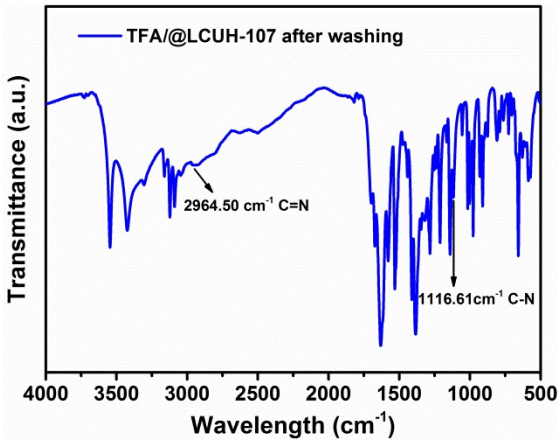

Figure S21. IR spectra (KBr pellet, cm^{-1}) of TFA/**LCUH–107W**.

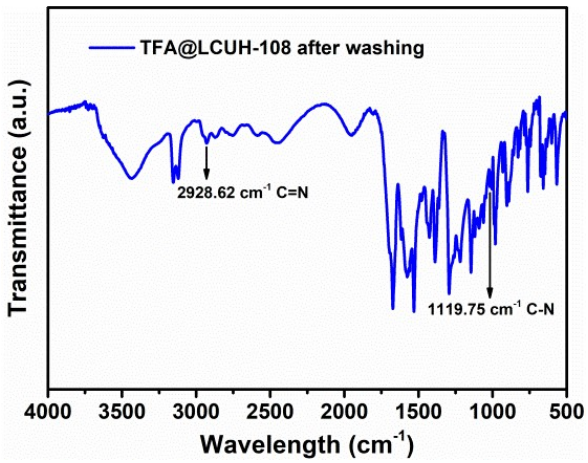

Figure S22. IR spectra (KBr pellet, cm^{-1}) of TFA@**LCUH–108W**.

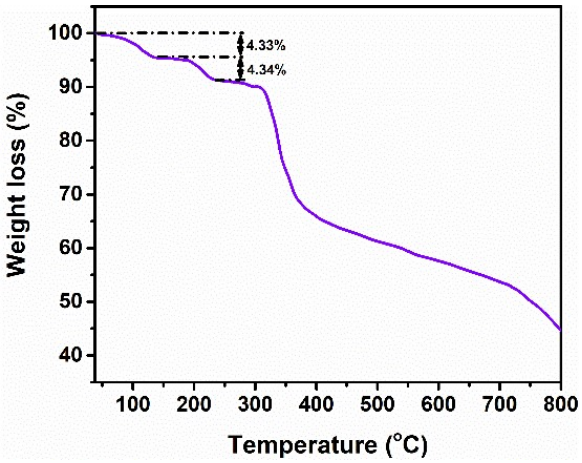

Figure S23. The TG curve of TFA/**LCUH–107W**.

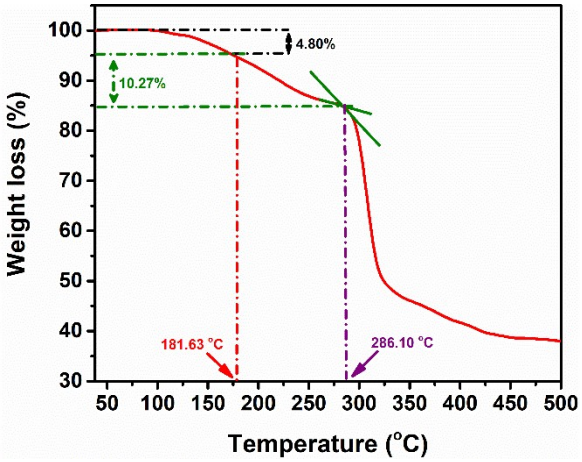

Figure S24. The TG curve of TFA@**LCUH–108W**.

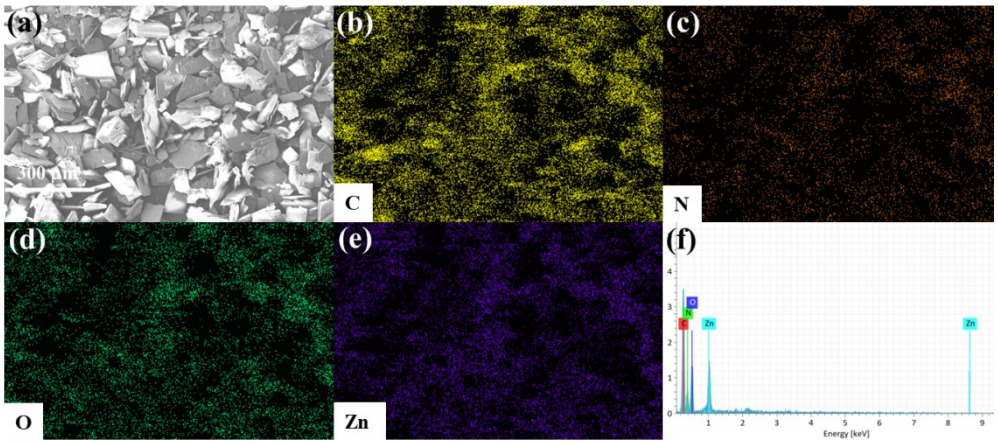

Figure S25. SEM image of TFA/**LCUH–107W** (a); energy–dispersive elemental mapping images for TFA/**LCUH–107W**: C (b), N (c), O (d), and Zn (e); (f) EDS image of TFA/**LCUH–107W**.

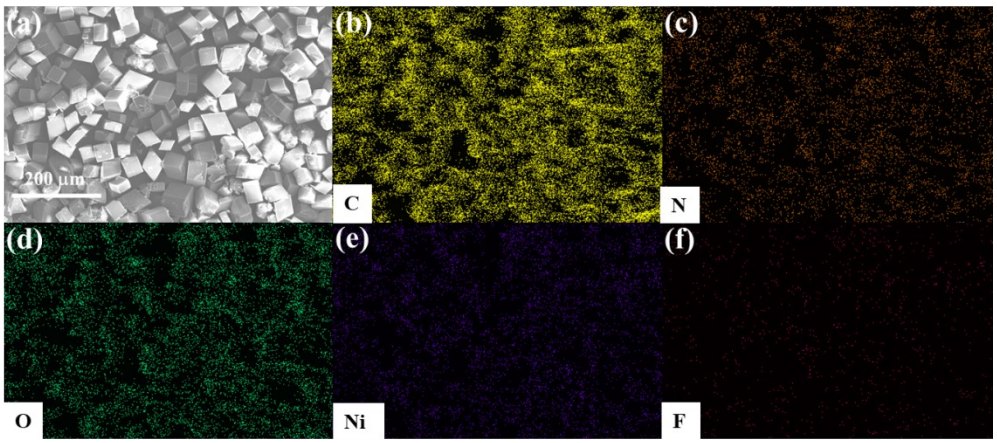

Figure S26. SEM image of TFA@**LCUH–108W** (a); energy–dispersive elemental mapping images for TFA@**LCUH–108W**: C (b), N (c), O (d), Ni (e), and F (f).

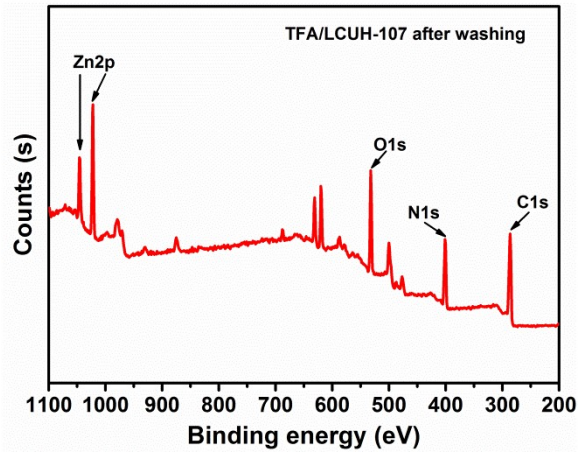

Figure S27. XPS spectra of TFA/**LCUH–107W**.

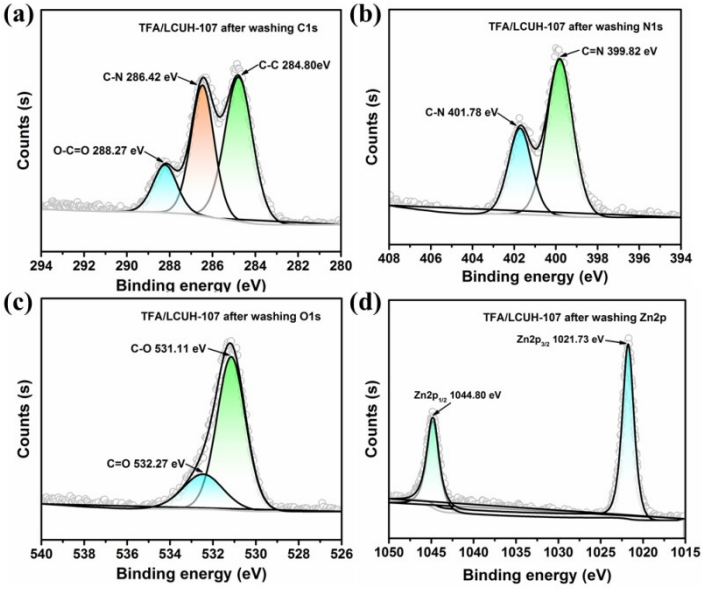

Figure S28. XPS spectra of (a) C1s, (b) N1s, (c) O1s, and (d) Zn2p in TFA/**LCUH–107W**.

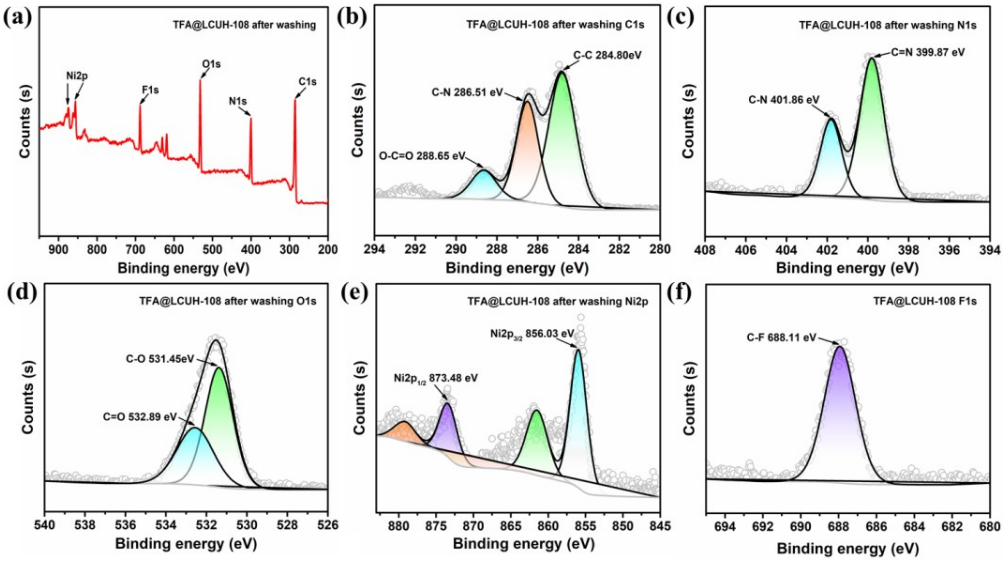

Figure S29. (a) XPS spectra of TFA@**LCUH–108W**. XPS spectra of (b) C1s, (c) N1s, (d) O1s, (e) Zn2p, and (f) F1s in TFA@**LCUH–108W**.

Table S9. Proton conductivities ($S \cdot cm^{-1}$) of **LCUH–107** at temperatures and different RHs

Temp (°C)	$\sigma(10^{-4}\,S \cdot cm^{-1})$ 75% RH	$\sigma(10^{-4}\,S \cdot cm^{-1})$ 85% RH	$\sigma(10^{-4}\,S \cdot cm^{-1})$ 93% RH	$\sigma(10^{-4}\,S \cdot cm^{-1})$ 100% RH
20	1.85	2.40	3.12	4.56
30	2.94	3.78	4.31	6.90
40	4.55	5.61	7.02	9.70
50	6.72	8.05	9.12	14.88
60	9.46	11.87	13.69	19.02
70	13.89	17.11	19.55	24.44
80	19.31	22.81	27.37	34.21

Table S10. Proton conductivities ($S \cdot cm^{-1}$) of TFA/**LCUH–107** at temperatures and different RHs

Temp (°C)	$\sigma(10^{-3}\,S \cdot cm^{-1})$ 75% RH	$\sigma(10^{-3}\,S \cdot cm^{-1})$ 85% RH	$\sigma(10^{-3}\,S \cdot cm^{-1})$ 93% RH	$\sigma(10^{-3}\,S \cdot cm^{-1})$ 100% RH
20	2.44	7.06	8.84	10.19
30	3.44	8.66	11.17	12.63
40	4.68	10.43	13.61	14.64
50	6.28	12.81	16.01	18.04
60	8.57	15.57	19.09	21.49
70	11.54	18.39	22.50	24.99
80	15.30	21.37	26.39	29.49

Table S11. Proton conductivities ($S \cdot cm^{-1}$) of **LCUH–108** at temperatures and different RHs

Temp (°C)	$\sigma(10^{-3}\,S \cdot cm^{-1})$ 45% RH	$\sigma(10^{-3}\,S \cdot cm^{-1})$ 60% RH	$\sigma(10^{-3}\,S \cdot cm^{-1})$ 75% RH	$\sigma(10^{-3}\,S \cdot cm^{-1})$ 85% RH	$\sigma(10^{-3}\,S \cdot cm^{-1})$ 93% RH	$\sigma(10^{-3}\,S \cdot cm^{-1})$ 100% RH
20	0.0835	0.304	0.661	1.75	3.248	3.926

30	0.119	0.379	0.885	2.413	4.137	4.86
40	0.167	0.545	1.113	2.844	4.978	5.579
50	0.233	0.67	1.401	3.389	6.011	6.76
60	0.328	0.86	1.781	4.37	7.079	8.184
70	0.421	1.092	2.275	5.399	8.274	9.423
80	0.558	1.394	2.883	6.126	9.653	11.961

Table S12. Proton conductivities ($S \cdot cm^{-1}$) of TFA@**LCUH–108** at temperatures and different RHs

Temp (°C)	**σ(10^{-2} S·cm^{-1}) 45% RH**	**σ(10^{-2} S·cm^{-1}) 60% RH**	**σ(10^{-2} S·cm^{-1}) 75% RH**	**σ(10^{-2} S·cm^{-1}) 85% RH**	**σ(10^{-2} S·cm^{-1}) 93% RH**	**σ(10^{-2} S·cm^{-1}) 100% RH**
20	0.265	0.585	0.638	0.833	5.278	7.986
30	0.379	0.761	0.840	1.173	6.260	9.427
40	0.484	1.005	1.107	1.564	7.465	11.04
50	0.603	1.250	1.438	1.729	8.877	13.33
60	0.775	1.573	1.803	2.345	9.660	15.36
70	0.952	1.841	2.281	2.945	10.808	18.27
80	1.196	2.281	2.784	3.732	12.225	20.53

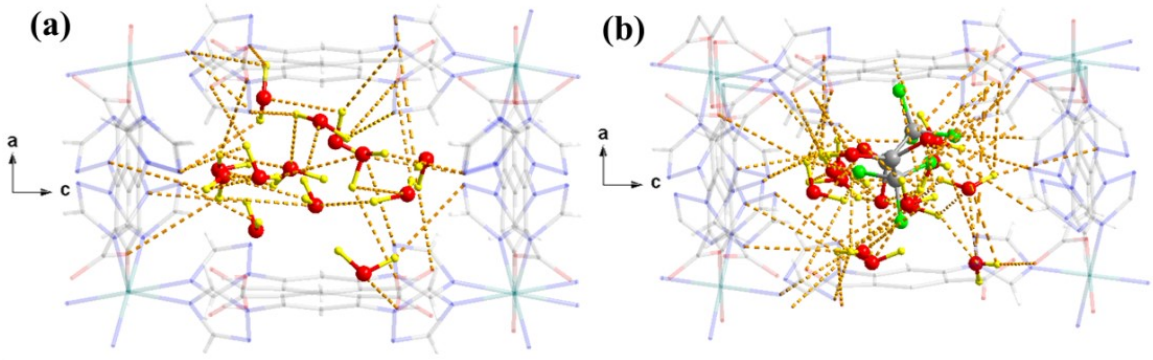

Figure S30. (a) Hydrogen–bonding interactions of **LCUH–108** with water molecules towards pore channels; (b) hydrogen–bonding interactions of **LCUH–108** with imidazole and water molecules towards pore channels.

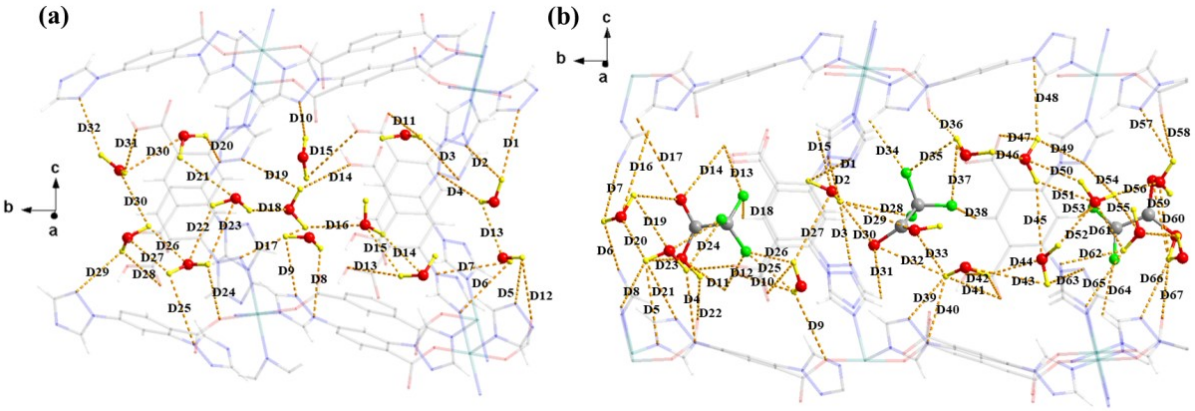

Figure S31. (a) Hydrogen–bonding interactions of **LCUH–108** with water molecules along pore channels; (b) hydrogen–bonding interactions of **LCUH–108** with imidazole and water molecules along pore channels.

Table S13. The hydrogen–bonding lengths of **LCUH–108** with water molecules (Figure S31a)

Bond	Length (Å)	Bond	Length (Å)	Bond	Length (Å)	Bond	Length (Å)
D1	2.808	**D2**	3.242	**D3**	3.501	**D4**	3.455
D5	2.989	**D6**	3.325	**D7**	3.198	**D8**	3.008
D9	3.265	**D10**	3.555	**D11**	3.293	**D12**	3.055
D13	3.246	**D14**	3.066	**D15**	3.172	**D16**	3.276
D17	3.186	**D18**	3.433	**D19**	3.507	**D20**	2.976
D21	3.437	**D22**	3.466	**D23**	3.398	**D24**	3.188
D25	3.426	**D26**	3.382	**D27**	3.279	**D28**	3.285
D29	3.401	**D30**	3.447	**D31**	3.356	**D32**	3.428

Table S14. The hydrogen–bonding lengths of TFA@**LCUH–108** with water molecules (Figure S31b)

Bond	Length (Å)	Bond	Length (Å)	Bond	Length (Å)	Bond	Length (Å)
D1	3.412	**D2**	3.256	**D3**	3.389	**D4**	3.052
D5	2.987	**D6**	2.930	**D7**	3.266	**D8**	3.249

D9	3.057	**D10**	3.340	**D11**	2.910	**D12**	3.076
D13	3.033	**D14**	2.921	**D15**	3.083	**D16**	3.013
D17	2.915	**D18**	3.082	**D19**	2.536	**D20**	2.549
D21	3.250	**D22**	2.397	**D23**	2.786	**D24**	2.397
D25	3.266	**D26**	3.049	**D27**	3.040	**D28**	2.698
D29	2.910	**D30**	2.883	**D31**	3.003	**D32**	3.189
D33	3.056	**D34**	3.112	**D35**	3.027	**D36**	3.250
D37	3.029	**D38**	3.076	**D39**	3.133	**D40**	2.625
D41	3.425	**D42**	3.375	**D43**	3.257	**D44**	3.066
D45	3.181	**D46**	3.077	**D47**	3.199	**D48**	3.456
D49	3.157	**D50**	3.098	**D51**	3.357	**D52**	3.266
D53	3.278	**D54**	3.182	**D55**	3.455	**D56**	3.256
D57	3.377	**D58**	3.428	**D59**	3.057	**D60**	3.399
D61	3.070	**D62**	3.054	**D63**	3.188	**D64**	3.375
D65	3.099	**D66**	3.500	**D67**	3.282		

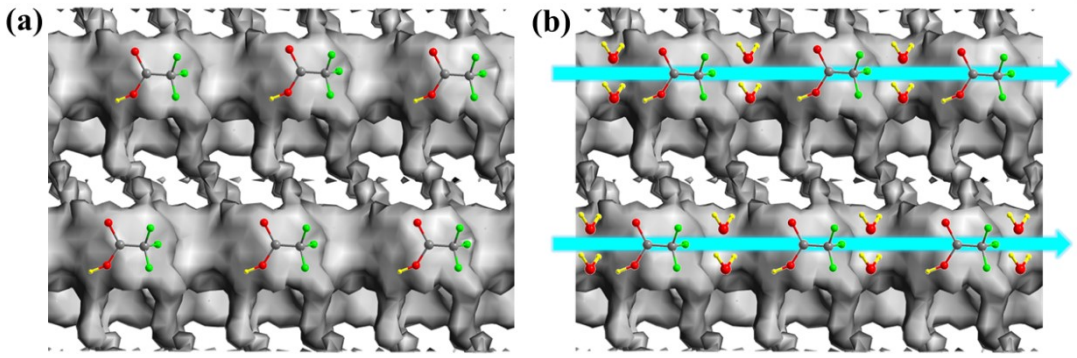

Figure S32. (a) Schematic diagram of TFA/**LCUH–107**. (b) Diagram of proton transport mechanism of TFA/**LCUH–107**.

Table S15. Comparison of proton conductivities between TFA/**LCUH–107** and TFA@**LCUH–108** with those reported in the literature.

Compounds	**σ (S·cm^{-1})**	**E_a (eV)**	**Condition**	**References**
Im@(NENU–3)	1.82×10^{-2}	0.57	70 °C, 90% RH	1

Im–Fe–MOF	1.21×10^{-2}	0.436	60 °C, 98% RH	2
Im@MOF–808	3.45×10^{-2}	0.25	65 °C, 99% RH	3
Im@Hf–UiO–66	1.15×10^{-2}	0.40	98 °C, 100% RH	4
Im@Hf–UiO–66–$(OH)_2$	1.32×10^{-2}	0.36	98 °C, 100% RH	4
Im@MOF–801–Hf	1.46×10^{-2}	0.53	100 °C, 98% RH	5
Nafion	5.00×10^{-2}	0.22	30 °C, 98% RH	6
PCMOF2½	2.10×10^{-2}	0.21	85 °C, 90% RH	7
IM–UiO–66–AS	1.54×10^{-1}	0.20	80 °C, 98% RH	8
PCMOF10	3.55×10^{-2}	0.4	70 °C, 95% RH	9
UiO–66$(SO_3H)_2$	8.40×10^{-2}	0.32	80 °C, 90% RH	10
VNU–15	2.90×10^{-2}	0.22	95 °C, 60% RH	11
MIP–202(Zr)	1.10×10^{-2}	0.22	90 °C, 95% RH	12
BUT–8(Cr)A	1.27×10^{-1}	0.11	80 °C, 100% RH	13
LCUH–107	3.42×10^{-3}	0.300	80 °C, 100% RH	this work
LCUH–108	1.20×10^{-2}	0.174	80 °C, 100% RH	this work
TFA/LCUH–107	2.95×10^{-2}	0.170	80 °C, 100% RH	this work
TFA@LCUH–108	2.05×10^{-1}	0.157	80 °C, 100% RH	this work

5. References.

1 Y. X. Ye, W. G. Guo, L. H. Wang, Z. Y. Li, Z. J. Song, J. Chen, Z. J. Zhang, X. C. Xiang, B. L. Chen, Straightforward Loading of Imidazole Molecules into Metal–Organic Framework for High Proton Conduction, *J. Am. Chem. Soc.* 2017, **139**, 15604–15607.

2 F. M. Zhang, L. Z. Dong, J. S. Qin, W. Guan, J. Liu, S. L. Li, M. Lu, Y. Q. Lan, Z. M. Su,

H. C. Zhou, Effect of Imidazole Arrangements on Proton–Conductivity in Metal–Organic Frameworks, *J. Am. Chem. Soc.* 2017, **139**, 6183–6189.

3 H. B. Luo, Q. Ren, P. Wang, J. Zhang, L.F. Wang, X. M. Ren, High Proton Conductivity Achieved by Encapsulation of Imidazole Molecules into Proton–Conducting MOF–808, *ACS Appl. Mater. Inter.* 2019, **11**, 9164–9171.

4 X. Chen, S. Z. Wang, S. H. Xiao, Z. F. Li, G. Li, High Protonic Conductivity of Three Highly Stable Nanoscale Hafnium(IV) Metal–Organic Frameworks and Their Imidazole Loaded Products, *Inorg. Chem.* 2022, **61**, 4938–4947.

5 H. M. Ren, Y. R. Liu, B. Y. Liu, Z. F. Li, G. Li, Comparative Studies on the Proton Conductivities of HafniumBased Metal–Organic Frameworks and Related Chitosan or Nafion Composite Membranes, *Inorg. Chem.* 2022, **61**, 9564–9579.

6 Y. Prykhodko, K. Fatyeyeva, L. Hespel and S. Marais, Progress in hybrid composite Nafion–based membranes for proton exchange fuel cell application, *Chem. Eng. J.*, 2021, **409**, 127329.

7 S. R. Kim, K. W. Dawson, B. S. Gelfand, J. M. Taylor and G. K. H. Shimizu, Enhancing Proton Conduction in a Metal–Organic Framework by Isomorphous Ligand Replacement, *J. Am. Chem. Soc.*, 2013, **135**, 963–966.

8 X. M. Li, J. Liu, C. Zhao, J. L. Zhou, L. Zhao, S. L. Li and Y. Q. Lan, Strategic hierarchical improvement of superprotonic conductivity in a stable metal organic framework system, *J. Mater. Chem. A*, 2019, **7**, 25165–25171.

9 P. Ramaswamy, N. E. Wong, B. S. Gelfand and G. K. H. Shimizu, A Water Stable Magnesium MOF That Conducts Protons over 10^{-2} S cm^{-1}, *J. Am. Chem. Soc.*, 2015, **137**, 7640–7643.

10 W. J. Phang, H. Jo, W. R. Lee, J. H. Song, K. Yoo, B. S. Kim and C. S. Hong, Superprotonic Conductivity of a UiO–66 Framework Functionalized with Sulfonic Acid Groups by Facile Postsynthetic Oxidation, *Angew. Chem. Int. Ed.*, 2015, **54**, 5142–5146.

11 T. N. Tu, Phan, N. Q.; Vu, T. T.; Nguyen, H. L.; Cordova, K. E.; Furukawa, H. High proton conductivity at low relative humidity in an anionic Fe–based metal organic framework, *J. Mater. Chem. A.*, 2016, **4**, 3638–3641.

12 F. Yang, G. Xu, Y. Dou, B. Wang, H. Zhang, H. Wu, W. Zhou, J. R. Li and B. Chen, A flexible metal–organic framework with a high density of sulfonic acid sites for proton conduction, *Nat. Energy*, 2017, **2**, 877–883.